Synthesis and Site Structure of a Replica Platinum−Carbon Composite Formed Utilizing Ordered Mesopores of Aluminum-MCM-41 for Catalysis in Fuel Cells

Kazuki Oka,[†] Yoshiyuki Shibata,[‡] Takaomi Itoi,[§] and Yasuo Izumi*,[†]

Department of Chemistry, Graduate School of Science, Department of Nanomaterial Science, Graduate School of Advanced Integration Science, and Department of Mechanical Engineering, Graduate School of Engineering, Chiba University, Yayoi 1-33, Inage-ku, Chiba 263-8522, Japan

Received: October 16, 2009

Platinum nanoparticles have been reported with mean sizes between 1.5 and 7 nm supported on carbon. The contact between Pt nanoparticles and C has never been controlled and monitored nanoscopically. In this paper, stable Pt nanoparticles with a mean size of 1.2 nm were synthesized embedded on/in a C matrix catalytically produced from acetylene over the Pt nanoparticles. The replica Pt−C composite was synthesized inside of the ordered mesopores (2.7 nm) of Al-MCM-41 followed by removal of the template. The contact between the Pt nanoparticle and C was experimentally observed by high-energy resolution Pt L_2-edge XANES spectra tuned to 11065.7 eV, at a lower energy by 5 eV than the Pt $L\beta_1$ peak top for the replica Pt−C pressed to electrolyte polymer (Nafion). The spectra were nicely reproduced in a theoretical spectrum using ab initio multiple scattering calculations for the interface Pt site between cuboctahedral Pt_{38} and graphite layers. Other Pt sites detected in state-selective Pt L_2-edge XANES were exclusively metallic for replica Pt−C/Nafion either in air or in H_2. The thus-characterized replica Pt−C composite was tentatively tested as a cathode of a H_2−air polymer electrolyte fuel cell in comparison to commercial 20 wt % Pt/Vulcan XC-72 as the cathode. The improvement of Pt dispersion stabilized on/in a C matrix, effective contact of Pt with C, and diffusion of O_2 in a few nanometers of replica Pt−C powder was suggested.

Introduction

The control of platinum nanoparticle size between 1.5 and 7 nm supported on carbon is essential in the application to fuel cells[1] and detoxification of exhaust gas from automobiles.[2] Pt nanoparticles on C nanofibers (mean Pt size of 1.7−4 nm),[3,4] C nanotubes (mean Pt size of 2−6.7 nm),[4–10] ordered mesoporous C (mean Pt size of 1.5−3 nm),[11–13] C powder (mean Pt size of 1.6−4.8 nm),[14–17] and spherical C (mean Pt size of 2.9 nm)[18] and Pt monolayer on nanoparticles of other metals[19] have been synthesized in narrow particle size distribution.

The polymer electrolyte fuel cell (PEFC) is expected to be a portable and compact power source to start at atmospheric temperature and be operated at lower than 373 K for automobile and home use.[20] In the design of PEFCs, the cathode catalyst for the oxygen reduction reaction $(O_2 + 4H^+ + 4e^- \rightarrow 2H_2O)$ is most critical because the physical contact of Pt with C (electric contact), the electrolyte (wet polymer to transport protons), and oxygen gas needs to be enabled at the same time.[1] The morphologic effects of Pt nanoparticles, films, and alloys on the oxygen reduction reaction were reported.[1,21] In contrast that the Pt nanoparticles have been formed on various types of controlled C materials,[3–17] the electric contact of Pt with C has never been controlled and monitored nanoscopically.

In this work, the contact of Pt with C was controlled based on the idea of catalytic acetylene decomposition over Pt nanoparticles in a narrow size distribution centered at 1.2 nm formed inside of Al-exchanged ordered mesoporous silica Al-MCM-41 to produce Pt−C composites in mesopores. The replica Pt−C composite was separated via the removal of Al-MCM-41 using hydrofluoric acid. The synthesis of the replica Pt−C composite was monitored using high-resolution transmission electron microscope (TEM), X-ray diffraction (XRD), and Brunauer, Emmett, and Teller (BET) adsorption of N_2. The local structure and heterogeneity of Pt sites were analyzed based on conventional Pt L_3- and L_2-edge X-ray absorption fine structure (XAFS) and state-selective Pt $L\beta_1$-selecting Pt L_2-edge XAFS, respectively. State-selective XAFS was applied to Pt catalysts for the first time.

The Pt nanoparticles in a narrow size distribution centered at 1.2 nm are advantageous to use most of the Pt sites (80%) for oxygen reduction;[1] however, mass-specific activity for oxygen reduction is still under debate and/or critically depends on reaction conditions. The rate constant values were nearly constant for mean Pt particles between 1.6 and 4.8 nm on C.[17] The mass-specific activity gradually decreased when the mean Pt particle size decreased from 30 to 1 nm[22] or reached a maximum at 3.5 nm.[23] The instability of Pt particles as small as 1 nm was suggested to be transformed into amorphous and less active.[9] In this paper, stabilization of Pt nanoparticles (mean 1.2 nm) was tried on/in a C matrix catalytically formed from acetylene in mesoporous space. The electronic structure of the interface Pt site between Pt nanoparticles and C was investigated. The replica Pt−C was pressed as a tentative cathode catalyst of membrane electrolyte assembly (MEA).

Experimental Section

Synthesis. Ten milliliters of an 8.4 mM aqueous solution of tetraammineplatinum(II) hydroxide hydrate $Pt^{II}(NH_3)_4(OH)_2 \cdot 2H_2O$ (Strem Chemicals) and 1.0 g of Al-MCM-41 (molar ratio SiO_2/

* To whom correspondence should be addressed. E-mail: yizumi@faculty.chiba-u.jp. Phone and Fax: +81-43-290-3696.
† Graduate School of Science.
‡ Graduate School of Advanced Integration Science.
§ Graduate School of Engineering.

Analysis and Catalysis of a Replica 1.2 nm Pt−C Composite

J. Phys. Chem. C, Vol. 114, No. 2, 2010 **1261**

$Al_2O_3 = 0.9875/0.0125$, 1.11 wt % Al; Aldrich) were mixed and stirred at 353 K for 2 days. The suspension was filtered, washed, and heated in vacuum at 573 K for 2 h. The obtained powder (Pt−Al-MCM-41, 1.3 wt % Pt) was in a 30 mL min^{-1} H$_2$ (>99.99%; 101 kPa) flow at 573 K for 2 h and then in a 200 mL min^{-1} C$_2$H$_2$ (>98%) + N$_2$ (>99.999%) flow (molar ratio 1:9, total 101 kPa) at 973 K for 1 h. The obtained black powder (0.72 wt % Pt) was treated with 30 mL of hydrofluoric acid (15%; special grade, Wako Pure Chemical) to give the replica Pt−C composite (0.84 wt % Pt). Fortunately, in view of electric conductivity, amorphous C dissolved in hydrofluoric acid, and Pt−graphite was preferably obtained.[6,24] Somanathan et al. prepared Pt nanoparticles starting from hydrogen hexachloroplatinate(IV) in Al-MCM (molar ratio $SiO_2/Al_2O_3 = 0.995/0.005$) followed by calcination at 823 K. In 200 mL min^{-1} of C$_2$H$_2$ + N$_2$ flow (molar ratio 3:7), the start of C decomposition at 923 K, carbon nanotube formation between 973 and 1073 K, the maximum C decomposed at 1073 K, and preferable formation of graphitic sheets and amorphous C at 1173 K were reported.[6] The starting temperature of C decomposition and the maximum decomposed C yield were reproduced in this work, but we chose a relatively low temperature of 973 K for C$_2$H$_2$ decomposition to prevent the thermal growth of Pt nanoparticles.

Replica Pt−C powder (76 mg) was dispersed in 1.0 mL of 15% Nafion dispersion solution (DE2021-CS, Wako Pure Chemical) using ultrasonic treatment (85 W, 28 kHz) and was mounted on 190 μm thick C paper coated with polytetrafluoroethylene (TGP-H-060H, Chemix). Similarly, 25 mg of commercial 20 wt % Pt supported on C (Vulcan XC-72, Cabot) was dispersed on TGP-H-060H using a 5−10% Nafion dispersion solution. As a reference, mechanically dispersed Pt/Vulcan XC-72 on TGP-H-060H was also prepared. A 50 μm thick electrolyte polymer Nafion film (NR-212, Dupont; >95%; acid capacity > 9.2×10^{-4} equiv g^{-1}) was pressed with replica Pt−C/TGP-H-060H as the cathode and 20 wt % Pt/Vulcan XC-72/TGP-H-060H as the anode for MEA. Another MEA was made using the same Nafion film pressed with 20 wt % Pt/Vulcan XC-72/TGP-H-060H on both sides. The area of the electrode catalysts was 5 cm^2.

Characterization. Nitrogen adsorption measurements were performed at 77 K with the pressures between 1.0 and 90 kPa in a vacuum system connected to diffusion and rotary pumps (10^{-6} Pa) and equipped with a capacitance manometer (models CCMT-1000A and GM-2001, ULVAC). The samples were evacuated at 393 K for 2 h before measurements. High-resolution TEM images were taken using LaB$_6$ source TEM equipment (JEOL, Model JEM-4000FX) with an accelerating voltage of 400 kV. Samples were dispersed in ethanol (>99.5%, Wako Pure Chemical) and mounted on amorphous C-coated copper mesh (CU150 Mesh, JEOL).

XRD data were obtained using a Rigaku MiniFlex diffractometer at a Bragg angle of $2\theta_B = 2-10°$ for ordered mesopores and 10−75° for crystallites of C and Pt. The conditions involved were 30 kV and 15 mA, Cu Kα emission, and a nickel filter. The replica Pt−C powder and each intermediate composite during the synthesis were set in a dip of 18 × 2 × 1 mm^3 on glass plate to measure the electric conductivity with the two-point method.[25]

The powder samples for synchrotron X-ray measurements were prepared in the vacuum system (10^{-6} Pa) and transferred in situ to a Pyrex glass cell equipped with 25−50 μm thick Kapton (Dupont) windows on both sides. The samples in H$_2$, air, or argon were sealed with fire and transported to the beamline. The replica Pt−C powder was mounted on TGP-H-060H, as described above, but pressed to only one side of Nafion

(NR-212) for synchrotron X-ray study. The Nafion and protection polyester films (50 μm) were used as a window of Pyrex glass cells.

Conventional Pt L$_3$- and L$_2$-edge XAFS spectra were measured at 290 K in transmission mode in the Photon Factory at the High-Energy Accelerator Research Organization (Tsukuba, Japan) on beamlines 9C and 12C. The storage-ring energy was 2.5 GeV, and the ring current was between 450 and 250 mA. A Si(111) double-crystal monochromator and cylindrical double mirror were inserted into the X-ray beam path. The parallelness of the double crystals was set to 65% intensity and to the maximum flux using a piezo translator. The slit opening size was 1 mm × 1 mm in front of the I$_0$ ionization chamber. The I$_0$ and I$_t$ ionization chambers were purged with the mixture of Ar(15%) + N$_2$(85%) and Ar, respectively. The scan steps were ~7.8, ~0.46, and ~2.5 eV in the pre-edge, edge, and postedge regions, respectively. The accumulation time was 1−10 s for a data point. The Pt L$_3$- and L$_2$ absorption edge energy values were calibrated to 11562 and 13272.3 eV, respectively, for the spectra of Pt metal.[26,27]

State-selective Pt L$_2$-edge XAFS measurements were performed at 290 K at the beamline 37XU of SPring-8 (Sayo, Japan). The storage ring energy was 8 GeV at the top-up ring current of 100 mA. A Si(111) monochromator and rhodium-coated mirror were used. The undulator gap was optimized to maximize the X-ray beam flux at each data point. To stabilize the X-ray beam position on the surface of the sample, the monochromator stabilization mechanism was used.[28]

The Pt Lβ_1 emission spectra were measured using a home-made Rowland-type fluorescence spectrometer set at beamline 37XU.[28–30] A Johann-type spherically bent Ge(844) crystal (Saint-Gobain; curvature radius of 450 mm, $d = 0.57737$ Å) and NaI(Tl) scintillation counter (SC; Model SP-10, Oken) were mounted. The energy resolution of the fluorescence spectrometer was estimated to be 3.4 eV at Pt Lβ_1, including the contribution of the beamline. The apparent core−hole lifetime width for Pt Lβ_1-selecting XAFS was estimated to be 2.0 eV based on the formula[31]

$$\frac{1}{\Gamma_{App}{}^2} = \frac{1}{\Gamma_{Pt\ 3d_{3/2}}{}^2} + \frac{1}{\Gamma_{Pt\ 2p_{1/2}}{}^2}$$

The gas for the ion chamber was 30% N$_2$ and 70% He in front of the sample. The slit opening in the front of the ionization chamber was 0.3 mm (horizontal) × 1.0 mm (vertical). The sample was placed in a plane near horizontal, tilted by 6° toward the incident X-ray and by 7° toward the Ge crystal. The sample surface, Ge crystal, and slit in front of the SC were controlled on a Rowland circle (radius 225 mm) in the vertical plane. The openings of the receiving slit and the slit in front of the SC were 8.0 mm (h) × 0.1 mm (v). The sample and SC were covered with a lead plate housing, except for the X-ray paths.

With the excitation energy set to 13298.8 eV, Pt Lβ_1 emission (M$_4$ → L$_2$; $\theta_B = 75.895°$) spectra were measured. The scan step was ~0.58 eV, and the accumulation time was 60 s for a data point. The fluorescence spectrometer was tuned to each energy around the Pt Lβ_1 emission peak, and Pt L$_2$-edge XANES (X-ray absorption near edge structure) spectra were measured. The scan step was ~0.46 eV with an accumulation time of 40−60 s for a data point. The Pt Lβ_1 fluorescence energy value was calibrated to 11070.84 eV for the spectrum of Pt metal.[26,27] The energy positions of the monochromator and the fluorescence

spectrometer were reproduced within ±0.1 and ±0.2 eV, respectively.

Analyses. The XAFS data were analyzed with XDAP (XAFS Services International).[32] The pre-edge background was approximated by a modified Victoreen function $C_2/E^2 + C_1/E + C_0$. The background of the postedge oscillation was approximated by a smoothing spline function, calculated by an equation for the number of data points where k was the wavenumber of photoelectrons.

$$\sum_{i=1}^{\text{data\_points}} \frac{(\mu x_i - BG_i)^2}{\exp(-0.075k_i^2)} \leq \text{smoothing factor}$$

Multiple shell curve fit analyses were performed for the Fourier-filtered k^3-weighted EXAFS data in k and R space using empirical amplitude and phase shift parameters extracted from EXAFS of PtO_2 and Pt metal for Pt−O [bond distance R(Pt−O) = 0.1993 nm with the coordination number (N) of 6][33] and Pt−Pt bonds [R(Pt−Pt) = 0.2775 nm with the N of 12][4] based on reported crystal structures. The many-body reduction factor S_0^2 was assumed to be equal for the sample and reference. The goodness of fit was given as requested by the Committee on Standards and Criteria in X-ray Absorption Spectroscopy.

The Pt L_3- and L_2-edge XANES spectra were theoretically generated using ab initio calculation code FEFF 8.4,[34] operated in a self-consistent field and full multiple scattering modes. Theoretical calculations of Pt XANES were reported to clarify the Pt cluster size effect and spectral change upon H/CO adsorption.[35-37] The exchange−correlation potential of Hedin−Lundqvist was chosen and corrected by adding a constant shift of +1.0 eV to the Fermi level. The calculated potential was also corrected by adding a constant shift of −1.6 eV to the "pure imaginary optical potential" to compare to Pt $L\beta_1$-selecting Pt L_2-edge spectra, but no shift was given for comparison to conventional XANES. The energy of the theoretically generated spectrum was shifted by +4.7 eV to compare to conventional Pt $L_{3/2}$-edge spectra and Pt L_2-edge spectra tuned to the Pt $L\beta_1$ peak top (11070.7−11070.8 eV). Corresponding to the Pt L_2-edge spectra tuned to 11065.7 and 11075.4 eV, the energies of the theoretically generated spectra were shifted by 0 and +8.2 eV, respectively.

The Pt metal site model consisted of 38 atoms of a face-centered cubic (fcc) Pt metal cuboctahedron. Among the Pt atoms, N(Pt−Pt) values of 6, 8, and 24 atoms were 12, 9, and 6, respectively.[38] The central Pt atom in the (111) surface ($N =$ 9) was considered as a representative Pt site for calculations (Figure 1) compared to an average N of 7.6 for all of the Pt sites. A central Pt atom in the (111) surface was in vacuum or at the interface with 177 atoms of three layers of graphite [R(C−C) = 0.1418 nm]. The Pt−C bond length was varied between 0.16 and 0.22 nm based on the crystal structures of organometallic compounds.[39] Relatively long R(Pt−C) values of 0.320−0.359 nm were used in the calculation model of Pt_{37} on graphite.[40] The Pt L_2-edge spectrum tuned to 11065.7 eV for replica Pt−C/Nafion was best reproduced theoretically by setting the R(Pt−C) to 0.18 nm. Thus, the nearest Pt−C bond distance was fixed to 0.18 nm. Average R(Pt−C) and N values were 2.0 nm and 1.9, respectively, for seven Pt atoms at the interface (Figure 1).

Results

N_2 Adsorption, XRD, TEM, and Conductivity. The specific surface area (S_{BET}) of 970 m^2 g^{-1} for Al-MCM-41 decreased
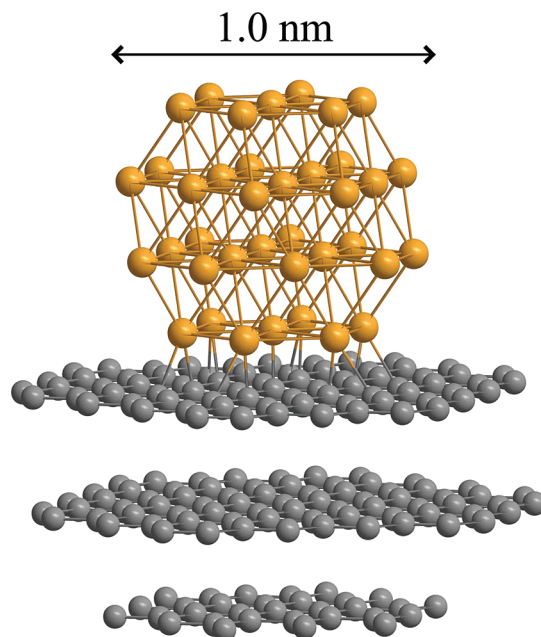

Figure 1. The Pt_{38} cluster model on three layers of graphite for XAFS analyses.

by 21% upon impregnation of Pt (Table 1). In contrast to this partial block of mesopores, the S_{BET} for Pt−Al-MCM-41 decreased by 95% after catalytic C_2H_2 decomposition, suggesting that a (nearly) complete block of mesopores by C formed. The loss of S_{BET} was recovered to 540 m^2 g^{-1} with the HF treatment (Table 1).

The regularity of the MCM-41 framework was monitored by XRD during the synthesis step of replica Pt−C. The distance between the pore and neighboring pore (a_0 of the unit cell) was 4.7 nm ($d_{100} = 4.1$ nm) for Al-MCM-41 (Table 1).[6,41] The value decreased to 4.5 nm ($d_{100} = 3.9$ nm) upon impregnation of Pt, in a similar trend to ref 6. In contrast, no peak was detected in XRD for Pt−C−Al-MCM-41 probably because the electron density of C formed in Al-MCM-41 mesopores was similar to that of the Al−SiO_2 template. The lower-angle peaks recovered at $d = 3.7$ and 3.2 nm for replica Pt−C composites, but the intensity was weaker compared to the peak for Pt−Al-MCM-41. No distinct peaks derived from the Pt or C crystallite were observed throughout the synthesis step of replica Pt−C. After a fuel cell test for 3 h, the replica Pt−C composite used as the cathode was re-examined by XRD. No peak was observed in the range of $2\theta_B = 10-75°$, suggesting the Pt particle size remained small.

The TEM image for replica Pt−C is depicted in Figure 2A. Darker dots of Pt particles are clearly observed between 0.38 and 3.33 nm (Figure 2C). The mean particle size is 1.2 nm, with a standard deviation of 0.5 nm. The mean size corresponds to a total of 66 atoms in one particle.[38] Most of the Pt particles are within the pore size of Al-MCM-41 (2.7 nm) (Figure 2C). The replica C is not clear in TEM images probably because the axis of replica Pt−C may randomly distribute, and the diameter of the rod/tube-like structure should be less than 3 nm dispersed over amorphous C coated on Cu mesh. However, the straight arrangement of darker Pt spots is observed, reminiscent of the ordered mesoporous structure of the Al-MCM-41 framework (Figure 2B).

The electric conductivity for Pt−Al-MCM-41 of less than 1 μS cm^{-1} dramatically increased to 263 mS cm^{-1} upon catalytic C_2H_2 decomposition (Table 1). The value was by 17% superior

Analysis and Catalysis of a Replica 1.2 nm Pt–C Composite

J. Phys. Chem. C, Vol. 114, No. 2, 2010 **1263**

TABLE 1: Physicochemical Characterization of Intermediate and Final Materials in the replica Pt–C Composite Synthesis

sample	specific S_{BET} (m² g⁻¹)	$R_{Pore-Pore}$ (nm)[a]	Pt loading (wt%)[b]	N_{Pt-Pt}[c]	N_{Pt-O} or N_{Pt-C}[c]	TEM[d] d_{Pt-Pt} (nm)	XRD[e]	electric conductivity (mS cm⁻¹)	ref
Al-MCM-41	970	4.7	–	–	–	–		<0.001	this work
Pt–Al-MCM-41	767	4.5	1.3	–	–	–		<0.001	this work
Pt–C–Al-MCM-41	35	n.p.[f]	0.72	5.1	2.1	–	n.p.[f]	263	this work
replica Pt–C	540	–	0.84	6.1	2.2	1.2	n.p.,[f] n.p.[f,g]	259	this work
Pt/Vulcan XC-72	–	–	20	12	–	–	4.8	224	this work
hexagonal Pt-block copolymer composite	18	30	74					2.5	25

[a] Distance from the center of the pore to the center of the neighboring pore based on XRD. [b] Based on the Pt L₃-edge jump value. [c] Coordination number based on the Pt L₃-edge EXAFS curve fit analysis. [d] Average particle size of Pt based on TEM image. [e] Average particle size of Pt based on XRD. [f] No peak detected. [g] Sample after PEFC cell test for 3 h.
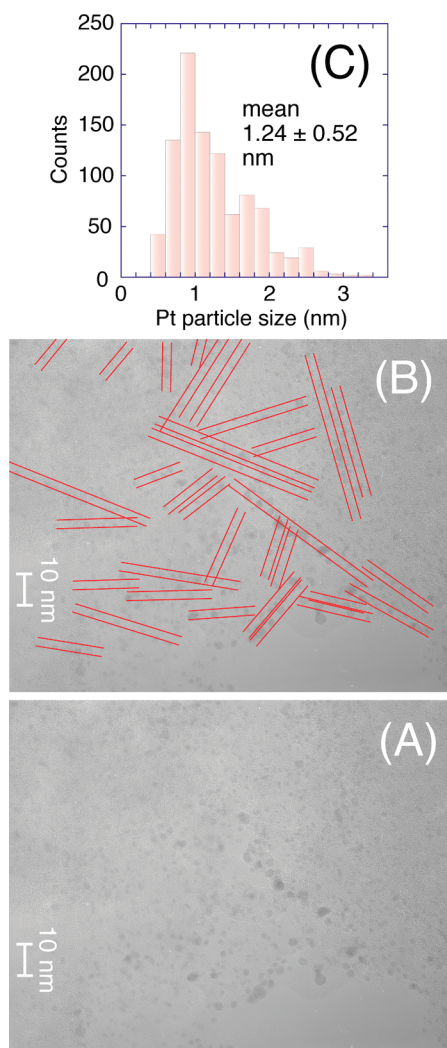

Figure 2. High-resolution TEM image for replica Pt–C (A). The internal size of mesopores of Al-MCM-41 was added in (B). The size distribution of the darker dots of Pt particles (C).

Figure 3. Normalized Pt L₃-edge XANES spectra for Pt–Al-MCM-41 (a), Pt–C–Al-MCM-41 (b), replica Pt–C in air (c), replica Pt–C/Nafion in air (d), Pt metal of 5 μm thickness (e), PtO₂ (f), and 20 wt % Pt/Vulcan XC-72/Nafion (g).

to that for 20 wt % Pt/Vulcan XC-72. The value for replica Pt–C (259 mS cm⁻¹) was comparable to that for Pt–C–Al-MCM-41 (Table 1).

Conventional XANES. Conventional Pt L₃-edge XANES spectra were measured during synthesis steps of the replica Pt–C composite (Figure 3). The peak positions of XANES for Pt–Al-MCM-41 (11565.7, 11580.5, and 11594.2 eV; spectrum (a)) were similar to those for Pt metal (spectrum (e)). The intensity of three postedge peaks was weaker for Pt–Al-MCM-41 compared to that for corresponding peaks for Pt metal, demonstrating that the Pt particles in Pt–Al-MCM-41 were on the nanometer scale.
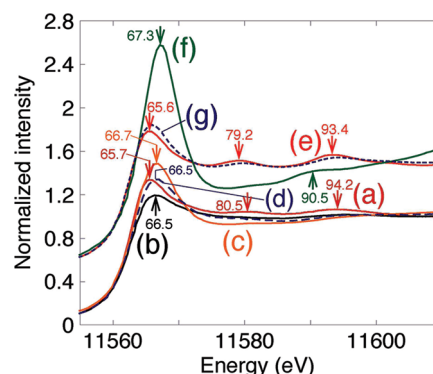
The peak at 11566.5 eV for Pt–C–Al-MCM-41 (spectrum (b)) became weaker and broader compared to that at 11565.7 eV in spectrum (a). An attempt was made to fit spectra (a) and (b) with theoretical spectra for a metallic Pt site or interface Pt site between the metal and graphite. It was difficult to fit because spectrum (a) seemed to be a mixture of metallic and oxidic Pt sites. Spectrum (b) seemed to be a mixture of metallic Pt and Pt at the interface with C. Instead, Pt Lβ₁-selecting XANES spectra were compared to theoretical data because the Pt state was selected and the spectral pattern was sharpened.[28,29,42–47]

The XANES spectrum for the replica Pt–C composite in air is shown in Figure 3c. The energy of first peak above the absorption edge (11566.7 eV) is intermediate between the peak at 11565.6 eV for the Pt metal (spectrum (e)) and the one at 11567.3 eV for PtO₂ (spectrum (f)). The first peak for spectrum (c) is more intense (1.47) than those for spectra (a) and (b) (1.33–1.19), and the postedge pattern of spectrum (c) became featureless. Thus, oxidation of part of metallic Pt in Pt–C–Al-MCM-41 was suggested after the removal of the Al-MCM-41 framework. In the XANES spectrum for Pt sites in replica Pt–C/Nafion in air (Figure 3d), the first peak above the absorption edge shifted down to 11566.5 eV, and the intensity decreased (1.34). The peak intensity was essentially identical to that for spectrum (a) (1.34 versus 1.33). No peak feature at 11590.5 eV for PtO₂ (spectrum (f)) was detected in spectrum (d). The postedge pattern of spectrum (d) was most like that of spectrum (b).

In comparison, a XANES pattern of 20 wt % Pt/Vulcan XC-72/Nafion (Figure 3g) corresponded exactly to that for Pt metal (spectrum (e)). The mean Pt particle size in the sample was 4.8 nm based on the peak width of XRD, much greater than that in the replica Pt–C composite (1.2 nm) and in less contact with Nafion.
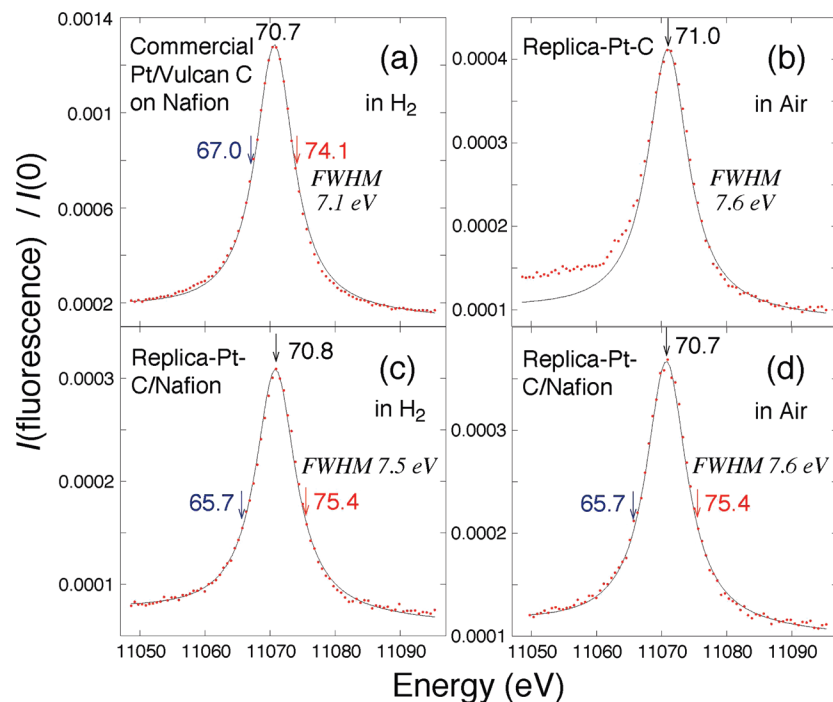
Figure 4. Pt Lβ_1 emission spectra for Pt/Vulcan XC-72/Nafion in H$_2$ (a), replica Pt−C in air (b), replica Pt−C/Nafion in H$_2$ (c), and replica Pt−C/Nafion in air (d). The arrows indicate tune energy values for Pt Lβ_1-selecting XAFS measurements (Figure 5).

X-ray Emission and State-Selective XANES. The Pt Lβ_1 emission peaks for replica Pt−C/Nafion in H$_2$ or in air appeared at 11070.7−11070.8 eV (Figure 4c, d), essentially identical to that for Pt metal (11070.84 eV). The emission peak for replica Pt−C powder in air was 11071.0 eV (spectrum (b)), shifted by +0.2 eV from that for Pt metal. The fwhm (full width at half-maximum) values were relatively greater (7.5−7.6 eV) for replica Pt−C/Nafion and replica Pt−C powder compared to 7.1−7.2 eV for standard Pt compounds and 20 wt % Pt/Vulcan XC-72/Nafion (spectrum (a)).

Then, Pt L$_2$-edge XANES spectra were measured (Figure 5B) tuned to the Pt Lβ_1 peak top (11070.7−11071.0 eV; the arrows in Figure 4). The absorption edge position progressively shifted from 13272.3 eV for Pt metal (spectrum (a)) to 13272.8 eV for replica Pt−C/Nafion in H$_2$ (spectrum (f)), 13272.9 eV for replica Pt−C/Nafion in air (spectrum (e)), or 13273.4 eV for replica Pt−C in air (spectrum (d)) and then to 13274.2 eV (PtO$_2$, spectrum (b)). Despite the gradual edge shift, postedge peaks appeared at almost the same position (13287−13289, 13302, 13312, and 13327 eV) for replica Pt−C/Nafion in H$_2$/in air and replica Pt−C in air (spectra (d)−(f)) as those for Pt metal (spectrum (a)). Thus, metallic Pt states were selected in replica Pt−C samples (as powder or on Nafion) in XANES spectra tuned to 11070.7−11071.0 eV.

Pt L$_2$-edge XANES spectra tuned to the lower-energy side of Pt Lβ_1 peaks (11065.7−11067.0 eV; the arrows in Figure 4) are shown in Figure 5A. The first intense peak at 13272.3−13273.3 eV above the absorption edge (spectra A(e), (f)) became weaker compared to the peaks in spectra tuned to the Pt Lβ_1 peak top (panel B(e), (f)). The absorption edge position for replica Pt−C/Nafion shifted from 13267.9 eV in H$_2$ to 13268.1 eV in air.

The postedge pattern for 20 wt % Pt/Vulcan XC-72/Nafion (Figure 5A(c)) resembled that of metallic Pt tuned to the Pt Lβ_1 peak top (Figure 5B(a)) if the spectrum B(a) shifted by 2.3 eV toward the lower-energy side. In contrast, the postedge pattern of spectra A(e) and (f) for replica Pt−C/Nafion became featureless in panel A and did not resemble that of metallic Pt
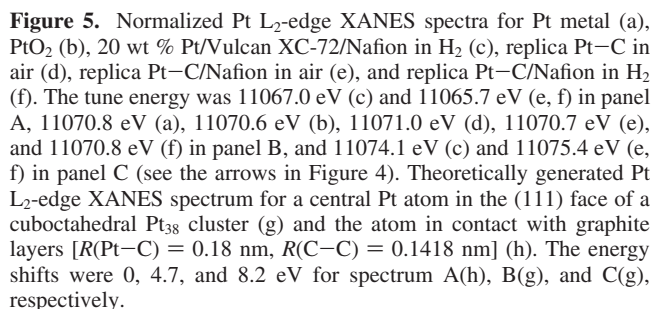
or PtO$_2$. The spectra (e) and (f) resembled theoretical spectra for the interface Pt atom between Pt metal and graphite (Figures 1 and 5A(h)) when the energy was shifted by −4.7 eV relative to XANES tuned to the Pt Lβ_1 peak top.

Next, Pt L$_2$-edge XANES spectra tuned to the higher-energy side of Pt Lβ_1 peaks (11074.1−11075.4 eV; the arrows in Figure 4) were measured for replica Pt−C/Nafion compared to 20 wt % Pt/Vulcan XC-72/Nafion (Figure 5C). The postedge pattern for spectra C(e) and (f) in Figure 5 resembled that of corresponding spectra tuned to the Pt Lβ_1 peak top (Figure 5B(e), (f)) if the spectra B(e) and (f) shifted by 3.5 eV toward the higher-energy side. The spectra (e) and (f) resembled theoretical spectra for a Pt atom in a Pt nanoparticle (Figure 5C(g)) when the energy was shifted by +3.5 eV relative to XANES tuned to the Pt Lβ_1 peak top (Figure 5B(g)). The absorption edge position for replica Pt−C/Nafion in air (13276.4 eV) was by 1.0 eV greater than that in H$_2$. Postedge peak shifts were within 1 eV toward the higher-energy side by switching the ambient gas from H$_2$ (spectrum (f)) to air (spectrum (e)).

The postedge pattern for 20 wt % Pt/Vulcan XC-72/Nafion (Figure 5C(c)) resembled that of metallic Pt tuned to the Pt Lβ_1 peak top (Figure 5B(a)) if the spectrum B(a) shifted by 2.7 eV toward the higher-energy side. The Pt Lβ_1 tune energy for spectrum C(c) was greater by 3.4 eV compared to the peak top. The Pt Lβ_1 tune energy for spectrum A(c) was smaller by 3.7 eV compared to the peak top, and the XANES peaks shift was 2.3 eV. The reduction of the tune energy difference versus the XAFS energy difference was 62−80% mainly due to the final-state relaxation effect.[48]

Discussion

Replica Pt−C Morphology. The Pt loading in Pt−Al-MCM-41 was 1.3 wt % after cation exchange and reduction in H$_2$ at 573 K (Table 1). The amount corresponds to 67.5 μmol of Pt substituting on the proton sites for 1 g of Al-MCM-41 (412 μmol of Al g^{-1}). Therefore, 32.8% (or 16.4%) of the proton

Analysis and Catalysis of a Replica 1.2 nm Pt−C Composite

J. Phys. Chem. C, Vol. 114, No. 2, 2010 **1265**

Figure 5. Normalized Pt L_2-edge XANES spectra for Pt metal (a), PtO_2 (b), 20 wt % Pt/Vulcan XC-72/Nafion in H_2 (c), replica Pt−C in air (d), replica Pt−C/Nafion in air (e), and replica Pt−C/Nafion in H_2 (f). The tune energy was 11067.0 eV (c) and 11065.7 eV (e, f) in panel A, 11070.8 eV (a), 11070.6 eV (b), 11071.0 eV (d), 11070.7 eV (e), and 11070.8 eV (f) in panel B, and 11074.1 eV (c) and 11075.4 eV (e, f) in panel C (see the arrows in Figure 4). Theoretically generated Pt L_2-edge XANES spectrum for a central Pt atom in the (111) face of a cuboctahedral Pt_{38} cluster (g) and the atom in contact with graphite layers [$R(Pt−C) = 0.18$ nm, $R(C−C) = 0.1418$ nm] (h). The energy shifts were 0, 4.7, and 8.2 eV for spectrum A(h), B(g), and C(g), respectively.

sites of Al-MCM-41 were exchanged to $[Pt(NH_3)_4]^{2+}$ species (or $[Pt(NH_3)_4(OH)]^+$ species). This exchange ratio was greater than values for Pt zeolites,[49] but the Pt amounts introduced into the samples were similar between 0.6 and 2.0 wt % due to the difference of Al concentrations, 10 − 12 wt % for zeolites[49] versus 1.11 wt % for Al-MCM-41 of this work.

The Pt loading for Pt−C−Al-MCM-41 was 0.72 wt % after catalytic C_2H_2 decomposition at 973 K over Pt particles in Al-MCM-41 (Table 1). Therefore, the C content in the Pt−C−Al-MCM-41 was 44.6%. If the pore volume for Al-MCM-41 was 0.6 cm³ g⁻¹,[41] the density of formed C was 2.25 g cm⁻³ (graphite), and catalytically formed C remained exclusively inside of the mesopores of Al-MCM-41 (HR-TEM), it is estimated that 60.5% of the mesopores was stuffed. No C rod/tube pushed out of mesopores was detected in TEM images for Pt−C−Al-MCM-41 (not shown). The S_{BET} value for Pt−Al-MCM-41 (767 m² g⁻¹) decreased by 95% after catalytic C_2H_2 decomposition (Table 1), supporting the effective block of mesopores. Only the external surface of Al-MCM-41 adsorbed N_2.

The Pt loading for replica Pt−C was 0.84 wt % after the removal of the Al-MCM-41 framework (Table 1). Therefore, 47.4% of Pt in Pt−C−Al-MCM-41 was lost during the washing with HF solution. The specific S_{BET} value for replica Pt−C

recovered as much as 540 m² g⁻¹ (Table 1). When the catalytic C_2H_2 decomposition temperature was 1073 K, thermally decomposed C was formed as a byproduct but could be separated from Pt−C−Al-MCM-41. The C content in the Pt−C−Al-MCM-41 was 66.0%. It is estimated that 143.9% of the mesopores for Al-MCM-41 were stuffed, suggesting excessive C was pushed out of mesopores. At 873 K, acetylene did not react either catalytically or thermally, consistent with ref 6.

When catalytic C_2H_2 decomposition was performed at 973 K in a closed circulation system or in a batch for Pt−Al-MCM-41, the decomposition was by 75% slower than that in the flow setup in this study. Formed H_2 due to C_2H_2 decomposition remained in the system and inhibited further C_2H_2 decomposition due to equilibrium. When MCM-41 or FSM-16 was used instead of Al-MCM-41, ion exchange was not applicable to introduce Pt species. Catalytic C_2H_2 decomposition was performed on the Pt nanoparticles, followed by HF treatment. The Pt content in obtained replica Pt−C was only 0.09 wt %.

The mean Pt particle size was 1.2 nm for replica Pt−C (Figure 2A, C). The average N value for Pt−Pt bonds by EXAFS (6.1; Table 1) suggested even smaller Pt nanoparticles.[38] This discrepancy is due to the contribution of $N_{Pt−O}$ or $N_{Pt−C}$. Pt−C−Al-MCM-41 and replica Pt−C samples both measured in air provided $N_{Pt−O}$ values of 2.1−2.2, including the undividable contribution of $N_{Pt−C}$ (Table 1) because the exterior of these Pt nanoparticles should be oxidized and/or carburized.

Pt Sites in Replica Pt−C. Partial oxidation of Pt sites was demonstrated in conventional Pt XANES for a replica Pt−C composite (Figure 3c). In contrast, a high energy resolution Pt L_2-edge XANES spectrum (Figure 5B(d)) tuned to the Pt $L\beta_1$ peak top (11071.0 eV; Figure 4b) preferably selected metallic Pt. The emission of Pt(IV) sites appeared at 11070.6 eV (not shown), and the spectral pattern tuned to 11070.6 eV for PtO_2 (Figure 5B(b)) was totally different from that in spectrum (d).

Conventional XANES for replica Pt−C/Nafion (Figure 3d) was similar to that for Pt metal (spectrum (e)) in the absorption edge region or that for Pt−C−Al-MCM-41 (spectrum (b)) in the postedge region. The XANES spectra tuned to the Pt $L\beta_1$ peak top for replica Pt−C/Nafion both in air and in H_2 exclusively detected metallic Pt sites (Figure 5B(e), (f)). The spectra resembled well theoretical spectrum B(g) generated for the surface Pt site on the (111) face of a cuboctahedral Pt_{38} cluster.

When the tune energy was on the lower energy side of the Pt $L\beta_1$ peak for replica Pt−C/Nafion (Figure 4c, d), the first intense peak at 13272.3−13273.3 eV became weaker (Figure 5A(e), (f)), suggesting greater occupation of the Pt 5d band. The spectra (e) and (f) resembled well theoretical spectrum 5A(h) calculated for the interface site between the Pt nanoparticle and graphite layers (Figure 1). Thus, interface Pt sites were predominantly selected in Pt L_2-edge XANES tuned to 11065.7 eV for replica Pt−C/Nafion, and negative charge transfer from C to Pt nanoparticles was suggested. However, the selective detection of interface Pt sites was unsuccessful for Pt(mean size 4.8 nm, Table 1)/Vulcan XC-72/Nafion. Only dominant metallic Pt sites appeared in XANES tuned to 11067.0 eV.

EXAFS, in general, provides statistical bonding information for Pt in a sample irradiated with X-ray. Therefore, Pt−C bonds are statistically preferably detectable for the Pt sites in Pt particles in a narrow size distribution centered at 1.2 nm compared to Pt sites in Pt particles of mean size 4.8 nm. Even so, the contribution of Pt−C bonds was statistically minor for replica Pt−C compared to that of Pt−Pt bonds (Figure 3a, b). High energy resolution XAFS in this work still provides

1266   *J. Phys. Chem. C, Vol. 114, No. 2, 2010*

Oka et al.

statistical bonding information; however, the information is specific for Pt sites corresponding to a lower Pt Lβ_1 emission energy of 11065.7 eV for replica Pt−C/Nafion (Figure 5A(e), (f)) and Pt/Vulcan XC-72/Nafion (Figure 5A(c)). Thus, the discussion is reasonable that Pt sites in contact with C were discriminated among smaller Pt particles in replica Pt−C/Nafion, and the XANES spectrum was compared to theoretical XANES data (Figure 5A(h)) for the interface Pt sites depicted in Figure 1. Even after being tuned to a lower Pt Lβ_1 energy of 11067.0 eV, the Pt−C interface site was not discriminated for Pt/Vulcan XC-72/Nafion because the site population was too small among Pt sites corresponding to lower Pt Lβ_1 emission energy. It is apparent that the reason was the greater mean Pt particle size and predominant population of Pt−Pt bonds in Pt/Vulcan XC-72/Nafion.

The XANES spectra tuned on the higher-energy side of Pt Lβ_1 (Figure 4c, d) for replica Pt−C/Nafion resembled the theoretical spectrum in Figure 5C(g) generated for surface the Pt site on the (111) face of Pt$_{38}$, shifted by +3.5 eV from spectrum B(g). This XANES shift was rationalized based on the difference of the fluorescence tune energy and the final-state relaxation effect. Metallic Pt state was selected in the XANES tuned to 11075.4 eV.

Due to the selection rule of the electronic transition (azimuthal quantum number $\Delta l = \pm 1$; total angular momentum $\Delta j = 0$, ± 1), the near-edge transition from L$_2$ (^{2}P$_{1/2}$) is limited to O$_4$ (^{2}D$_{3/2}$) at a deeper energy than O$_5$ (^{2}D$_{5/2}$), whereas those from L$_3$ (^{2}P$_{3/2}$) are both limited to O$_4$ and O$_5$.[49] This is the reason why the Pt L$_2$-edge white line is weaker than that in Pt L$_3$-edge spectra.[35] By changing the fluorescence tune energy between 11065.7 and 11075.4 eV (Figure 4c, d), electron-sufficient Pt sites in contact with C (Figure 5A(e), (f)) and relatively electron deficient Pt sites on/in Pt nanoparticles (Figure 5B, C(e), (f)) were discriminated, respectively. In contrast, a negligible difference was detected by switching the ambient gas from H$_2$ to air for replica Pt−C/Nafion, except for an absorption edge shift less of than 1 eV (Figure 5e, f). The shape resonance peak near the L$_3$-edge was reported, for example, by H adsorption on Pt.[35,36,49] One of the possibilities is that the antibonding level between Pt 5d$_{3/2}$ and the frontier level of the adsorbent was occupied for replica Pt−C/Nafion samples. It is also possible that a similar shape resonance peak appeared due to adsorbed H in H$_2$ and adsorbed O$_2$ in air. A technical reason may be that the XAFS measurements for Pt catalysts on Nafion were done as in a half-cell and no water was supplied/catalytically produced in samples during the measurements. The contact of Pt with C(solid) and Nafion(liquid) was found to be secure; however, Nafion in pure H$_2$ or air was not entirely mobile and thus may block the Pt/gas interface sites.

Implications to the PEFC Cathode Catalyst of Replica Pt−C. The electric conductivity for Pt−C−Al-MCM-41 was by 17% superior to that for conventional 20 wt % Pt/Vulcan XC-72 (Table 1) probably because catalytically formed C in mesopores was regularly oriented in the [001] direction of Al-MCM-41, despite the low Pt content in Pt−C−Al-MCM-41 (0.72 wt %). The comparable conductivity values for Pt−C−Al-MCM-41 and replica Pt−C (Table 1) were also understandable if we think that the nonconducting Al-MCM-41 part was removed, but regular orientation of the C rod/tube would be lost for the latter.

To enable 0.13 mg Pt cm^{-2} as the cathode catalyst, 76 mg of replica Pt−C (0.84 wt % Pt) was mounted on C paper versus 25 mg of 20 wt % Pt/Vulcan XC-72 on C paper (1 mg Pt cm^{-2}) (see Supporting Information). The greater amount of replica

Pt−C mounted caused difficulty in making physical contact of Pt with the electrolyte (wet polymer to transport protons) and oxygen gas at the same time.[1] Hence, to enable practical electric power generation using replica Pt−C catalyst, the Pt content in replica Pt−C powder should be increased to 20 wt % Pt typical for other commercial Pt/C catalysts while keeping the Pt particle size of 1.2 nm. One possibility is to increase the Al content from 1.11 wt % to the zeolite level of 10−12 wt % to augment the cationic Pt complexes exchanged. Another possibility is to utilize a three-dimensional mesoporous template, for example, MCM-48, to stabilize Pt nanoparticles on/in formed C in the three-dimensional mesopores. The advantage to synthesize metal particles in a narrow size distribution centered at ∼1 nm and to secure contact of the metal and C demonstrated in this paper can be applied to nonprecious metal−C catalysts, for example, cobalt or iron porphyrin decomposition[50] in mesoporous SiO$_2$-based templates. Carbonization of block copolymer self-assembled with Pt, Pb, and Nb species is another possibility to produce a Pt−C composite, as recently reported for an anode material resistive to CO poisoning.[51]

Conclusions

Pt nanoparticles introduced by cation group exchange and formed by heating in vacuum at 573 K inside of Al-MCM-41 catalyzed C$_2$H$_2$ decomposition to form a C rod/tube. The Al-MCM-41 template was removed with a 15% HF solution. Pt nanoparticles with a mean size of 1.2 nm were obtained embedded on/in the C matrix. The Pt loading was 0.84 wt %. The replica Pt−C synthesis procedure was supported by the changes of the specific S$_{BET}$ value from 767 m^2 g^{-1} for Pt−Al-MCM-41 to 35 m^2 g^{-1} for Pt−C−Al-MCM-41 and then to 540 m^2 g^{-1} for replica Pt−C. The Pt particles could not be monitored by XRD both before and after cathode catalytic tests in PEFC, suggesting the stability of 1.2 nm Pt particles embedded on/in the C matrix. The Pt sites in replica Pt−C pressed to Nafion were analyzed by Pt Lβ_1-selecting high energy resolution Pt L$_2$-edge XANES spectra. The first peak above the absorption edge for the spectra tuned to 11065.7 eV was weak, suggesting that interface Pt site received electron transfer from the C in contact. The high energy resolution XANES spectra for both interfacial Pt with C and metallic Pt sites were nicely reproduced in theoretical spectra generated using FEFF 8.4. The shape resonance peak in H$_2$ or in air was not certain probably because the antibonding levels were below the Fermi level or the shape resonance peaks for H and O$_2$ adsorbed were similar. Superior turnover numbers were tentatively evaluated for the Pt−C replica in the cathode compared to Pt/Valcun XC-72 due to the differences of effective contact of Pt with C versus Pt impregnation on C and the diffusion efficiency of O$_2$ in replica Pt−C powder (see Supporting Information).

Analysis and Catalysis of a Replica 1.2 nm Pt−C Composite

J. Phys. Chem. C, Vol. 114, No. 2, 2010 **1267**

Supporting Information Available: Supporting text and Figure S1 for PEFC tests. This material is available free of charge via the Internet at http://pubs.acs.org.

References and Notes

(1) Gasteiger, H. A.; Markovic, N. M. *Science* **2009**, *324* (5923), 48–49.

(2) Zhang, G.; Yamaguchi, T.; Kawakami, H.; Suzuki, T. *Appl. Catal., B* **1992**, *1* (3), L15–L20.

(3) Xuyen, N. T.; Jeong, H. K; Kim, G.; So, K. P.; An, K. H.; Lee, Y. H. *J. Mater. Chem.* **2009**, *19* (9), 1283–1288.

(4) Plomp, A. J.; Schubert, T.; Storr, U.; de Jong, H. P.; Bitter, J. H. *Topics Catal.* **2009**, *52* (4), 424–430.

(5) Du, H. Y.; Wang, C. H.; Hsu, H. C.; Chang, S. T.; Chen, U. S.; Yen, S. C.; Chen, L. C.; Shih, H. C.; Chen, K. H. *Diamond Relat. Mater.* **2008**, *17* (4/5), 535–541.

(6) Somanathan, T.; Pandurangan, A. *J. Porous Mater.* **2009**, *16* (4), 459–464.

(7) Saha, M. S.; Li, R.; Ye, S. *Electrochem. Commun.* **2009**, *11* (2), 438–441.

(8) Chen, C.; Chen, M.; Yu, H.; Lu, S.; Chen, C. *Jpn. J. Appl. Phys.* **2008**, *47* (4), 2324–2329.

(9) Sun, Y.; Zhuang, L.; Lu, J.; Hong, X.; Liu, P. *J. Am. Chem. Soc.* **2007**, *129* (50), 15465–15467.

(10) Sun, C.; Chen, L.; Su, M.; Hong, L.; Chyan, O.; Hsu, C.; Chen, K.; Chang, T.; Chang, L. *Chem. Mater.* **2005**, *17* (14), 3749–3753.

(11) Hayashi, A.; Kitajima, K.; Miyamoto, J.; Yagi, I. *Chem. Lett.* **2009**, *38* (4), 346–347.

(12) Wikander, K.; Hungria, A. B.; Midgley, P. A.; Palmqvist, E. C.; Holmberg, K.; Thomas, J. M. *J. Colloid Interface Sci.* **2007**, *305* (1), 204–208.

(13) Joo, S. H.; Choi, S. J.; Oh, I.; Kwak, J.; Liu, Z.; Terasaki, O.; Ryoo, R. *Nature* **2001**, *412* (6843), 169–172.

(14) Hui, C. L.; Li, X. G.; Hsing, I. M. *Electrochim. Acta* **2005**, *51* (4), 711–719.

(15) Prabhuram, J.; Wang, X.; Hui, C. L.; Hsing, I. M. *J. Phys. Chem. B* **2003**, *107* (40), 11057–11064.

(16) Wikander, K.; Ekström, H.; Palmqvist, A. E. C.; Lindbergh, G. *Electrochim. Acta* **2007**, *52*, 6848–6855.

(17) Yano, H.; Inukai, J.; Uchida, H.; Watanabe, M.; Babu, P. K.; Kobayashi, T.; Chung, J. H.; Oldfield, E.; Wieckowski, A. *Phys. Chem. Chem. Phys.* **2006**, *8*, 4932–4939.

(18) Ng, Y. H.; Ikeda, S.; Harada, T.; Higashida, S.; Sakata, T.; Mori, H.; Matsumura, M. *Adv. Mater.* **2007**, *19* (4), 597–601.

(19) Zhang, J.; Lima, H. B.; Shao, M. H.; Sasaki, K.; Wang, J. X.; Hanson, J.; Adzic, R. R. *J. Phys. Chem. B* **2005**, *109* (48), 22701–22704.

(20) Service, R. F.; Voss, D. *Science* **1999**, *285* (5428), 682–685.

(21) Lim, B.; Jiang, M.; Camargo, P. H. C.; Cho, E. C.; Tao, J.; Lu, X.; Zhu, Y.; Xia, Y. *Science* **2009**, *324* (5932), 1302–1305.

(22) Mayrhofer, K. J. J.; Blizanac, B. B.; Arenz, M.; Stamenkovic, V. R.; Ross, P. N.; Markovic, N. M. *J. Phys. Chem. B* **2005**, *109* (30), 14433–14440.

(23) Kinoshita, K. *J. Electrochem. Soc.* **1990**, *137* (3), 845–848.

(24) Wei, L.; Wang, B.; Wang, Q.; Li, L.; Yang, Y.; Chen, Y. *J. Phys. Chem. C* **2008**, *112* (45), 17567–17575.

(25) Warren, S. C.; Messina, L. C.; Slaughter, L. S.; Kamperman, M.; Zhou, Q.; Gruner, S. M.; DiSalvo, F. J.; Wiesner, U. *Science* **2008**, *320* (5884), 1748–1752.

(26) Bearden, J. A. *Rev. Mod. Phys.* **1967**, *39* (1), 78–124.

(27) Zschornack, G. *Handbook of X-ray Data*; Springer: Berlin/Heidelberg, Germany, 2007.

(28) Izumi, Y.; Obaid, D. M.; Konishi, K.; Masih, D.; Takagaki, M.; Terada, Y.; Tanida, H.; Uruga, T. *Inorg. Chim. Acta* **2008**, *361*, 1149–1156.

(29) Izumi, Y.; Nagamori, H.; Kiyotaki, F.; Masih, D.; Minato, T.; Roisin, E.; Candy, J. P.; Tanida, H.; Uruga, T. *Anal. Chem.* **2005**, *77* (21), 6969–6975.

(30) Izumi, Y.; Masih, D.; Roisin, E.; Candy, J. P.; Tanida, H.; Uruga, T. *Mater. Lett.* **2007**, *61*, 3833–3936.

(31) de Groot, F. M. F.; Krisch, M. H.; Vogel, J. *Phys. Rev. B: Condens. Matter* **2002**, *66*, 195112/1–195112/7.

(32) Vaarkamp, M.; Linders, H.; Koningsberger, D. XDAP, version 2.2.7 (2006); XAFS Services International: Woudenberg The Netherlands.

(33) Siegel, S.; Hoekstra, H. R.; Tani, B. S. *J. Inorg. Nucl. Chem.* **1969**, *31*, 3803–3807.

(34) Ankudinov, L.; Ravel, B.; Rehr, J. J.; Condradson, S. D. *Phys. Rev. B* **1998**, *58*, 7565–7576.

(35) Ankudinov, A. L.; Rehr, J. J.; Low, J. J.; Bare, S. R. *J. Synchrotron Radiat.* **2001**, *8*, 578–580.

(36) Bazin, D.; Sayers, D.; Rehr, J. J.; Mottet, C. *J. Phys. Chem. B* **1997**, *101* (27), 5332–5336.

(37) Safonova, O. V.; Tromp, M.; Bokhoven, J. A. v.; de Groot, F. M. W.; Evans, J.; Glatzel, P. *J. Phys. Chem. B* **2006**, *110* (33), 16162–16164.

(38) Humbolt, F.; Didillon, D.; Lepeltier, F.; Candy, J. P.; Corker, J.; Clause, O.; Bayard, F.; Basset, J. M. *J. Am. Chem. Soc.* **1998**, *120* (1), 137–146.

(39) Terheijiden, J.; Van Koten, G.; Van Beek, J. A. M.; Vriesema, B. K.; Kellogg, R. M.; Zoutberg, M. C.; Stam, C. H. *Organometallics* **1987**, *6*, 89–93.

(40) Wang, L.; Johnson, D. D. *J. Am. Chem. Soc.* **2007**, *129* (12), 3658–3664.

(41) Kruk, M.; Jaroniec, M.; Kim, J. M.; Ryoo, R. *Langmuir* **1999**, *15* (16), 5279–5284.

(42) Glatzel, P.; Bergmann, U. *Coord. Chem. Rev.* **2005**, *249*, 65–95.

(43) de Groot, F. *Chem. Rev.* **2001**, *101* (6), 1779–1808.

(44) Izumi, Y.; Nagamori, H. *Bull. Chem. Soc. Jpn.* **2000**, *73* (7), 1581–1587.

(45) Izumi, Y.; Kiyotaki, F.; Minato, T.; Seida, Y. *Anal. Chem.* **2002**, *74* (15), 3819–3823.

(46) Izumi, Y.; Kiyotaki, F.; Seida, Y. *J. Phys. Chem. B* **2002**, *106* (7), 1518–1520.

(47) Izumi, Y.; Masih, D.; Aika, K.; Seida, Y. *J. Phys. Chem. B* **2005**, *109* (8), 3227–3232.

(48) Izumi, Y.; Glaser, T.; Rose, K.; McMaster, J.; Basu, P.; Enemark, J. H.; Hedman, B.; Hodgson, K. O.; Solomon, E. I. *J. Am. Chem. Soc.* **1999**, *121* (43), 10035–10046.

(49) Koningsberger, D. C.; de Graaf, J.; Mojet, B. L.; Ramaker, D. E.; Miller, J. T. *Appl. Catal., A* **2000**, *191*, 205–220.

(50) Bashyam, R.; Zelenay, P. *Nature* **2006**, *443* (7107), 63–66.

(51) Orilall, M. C.; Matsumoto, F.; Zhou, Q.; Sai, H.; Abruña, H. D.; DiSalvo, F. J.; Wiesner, U. *J. Am. Chem. Soc.* **2009**, *131* (26), 9389–9395.